JACS
JOURNAL OF THE AMERICAN CHEMICAL SOCIETY

Article

pubs.acs.org/JACS

Transfer of Chirality from Molecule to Phase in Self-Assembled Chiral Block Copolymers

Rong-Ming Ho,*[,†,∥] Ming-Chia Li,[†] Shih-Chieh Lin,[†] Hsiao-Fang Wang,[†] Yu-Der Lee,[†] Hirokazu Hasegawa,[‡] and Edwin L. Thomas[§]

[†]Department of Chemical Engineering, National Tsing Hua University, Hsinchu 30013, Taiwan

[∥]Frontier Research Center on Fundamental and Applied Sciences of Matters, National Tsing Hua University, Hsinchu 30013, Taiwan

[‡]Department of Polymer Chemistry, Kyoto University, Kyoto 615-8510, Japan

[§]Department of Materials Science and Engineering, Institute for Soldier Nanotechnologies, Massachusetts Institute of Technology, Cambridge, Massachusetts 02139, United States

Supporting Information

ABSTRACT: Here, we report the mechanisms of chiral transfer at various length scales in the self-assembly of enantiomeric chiral block copolymers (BCPs*). We show the evolution of homochirality from molecular chirality into phase chirality in the self-assembly of the BCPs*. The chirality of the molecule in the BCP* is identified from circular dichroism (CD) spectra, while the handedness of the helical conformation in the BCP* is determined from a split-type Cotton effect in vibrational circular dichroism spectra. Microphase separation of the BCP* is exploited to form a helical (H*) phase, and the handedness of helical nanostructure in the BCP* is directly visualized from transmission electron microscopy tomography. As examined by CD and fluorescence experiments, significant induced CD signals and a bathochromic shift of fluorescence emission for the achiral perylene moiety as a chemical junction of the BCPs* can be found while the concentration of the BCPs* in toluene solution is higher than the critical micelle concentration, suggesting a twisting and shifting mechanism initiating from the microphase-separated interface of the BCPs* leading to formation of the H* phase from self-assembly.

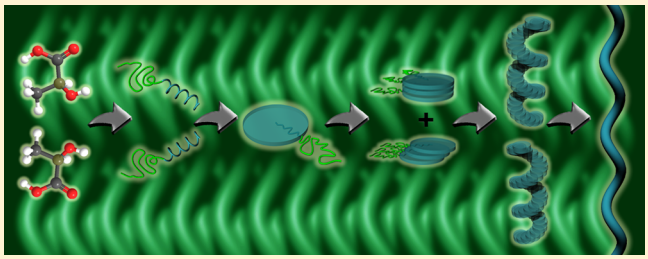

INTRODUCTION

Self-assembly involves spontaneous organization of molecules or macromolecules into stable, well-defined aggregates by secondary interactions (noncovalent forces).[1,2] Nature uses the self-assembly of molecules and supramolecules for structuring substances. Biological architectures are established by the interplay among secondary interactions, which forms various organizations.[3] Of them, helical morphologies are the most fundamental and interesting. The chirality of compounds has been identified as one of the main origins of formation of helical textures.[4−8] Block copolymers (BCPs) can self-assemble into bulk periodic nanostructures.[9−12] Hierarchical superstructures with a helical sense resulting from the self-assembly of amphiphilic BCPs that contain a charged chiral block can be obtained, suggesting that chirality participates importantly in formation of helical nanostructures.[13] Several years ago, a chiral BCP composed of chiral entities (denoted as BCP*), polystyrene-*block*-poly(L-lactide) (PS-PLLA), was designed for self-assembly. Twisted morphologies in the self-assembled phase of PS-PLLA prove formation of a helical (H*) phase.[14] This novel phase with hexagonally packed PLLA helical nanostructures in a PS matrix was thus defined as a H* phase with the *P*622 space group.[15] In nature, homochiral evolution is critical for key molecular processes, such as communication, replication, and enzyme catalysis, and relies on a delicate balance between molecular and supramolecular chirality.[16−19] Through the design and synthesis of molecules or supramolecules and the operation of self-assembly, the mechanisms of chiral transfer at different length scales can be understood. This biomimicking process may provide supporting information to disclose the mysteries of morphological evolution from the molecular level.

In this study, a methodology for systematic studies of the transfer of chirality from the molecular level to phase scale is established using polylactide-containing BCPs* for self-assembly. As identified by circular dichroism (CD) and vibrational circular dichroism (VCD), opposite chiral entities (i.e., configurational chirality) on the backbone of chiral blocks (i.e., main-chain chirality) construct the PLLA and poly(D-lactide) (PDLA) chains as helical conformations with preferential left- and right-handedness (i.e., conformational chirality), respectively, due to intramolecular interaction. By taking advantage of the intermolecular interaction, self-

Received: April 12, 2012
Published: May 23, 2012

   dx.doi.org/10.1021/ja303513f | J. Am. Chem. Soc. 2012, 134, 10974−10986

Table 1. Characterization of Polylactide Homopolymers, Polylactide-Containing BCPs, and Polylactide-Containing BCPs with a Perylene Bisimide Junction

sample	M_n^{PS} (g/mol)[a]	M_n^{PLA} (g/mol)[a]	N_{PS}[a]	N_{PLA}[a]	M_n^{total} (g/mol)[a]	PDI[b]	f_{PLA}^{vc}
PLLA	15 700	109			15 700	1.06	
PDLA	15 700	109			15 700	1.04	
PLA	14 800	102			14 800	1.29	
PS-PLLA	23 600	15 600	226	108	39 200	1.25	0.35
PS-PDLA	24 000	19 000	230	131	43 000	1.25	0.39
PS-PLA	23 000	14 800	221	102	37 800	1.31	0.35
PS-*perylene*-PLLA	24 900	7900	239	55	32 800	1.26	0.21
PS-*perylene*-PLLA	32 000	20 800	307	144	52 800	1.08	0.35
PS-*perylene*-PDLA	24 900	7200	239	50	32 100	1.24	0.19
PS-*perylene*-PDLA	32 000	21 800	307	151	53 800	1.12	0.35
PS-*perylene*-PLA	24 900	7300	239	51	32 200	1.21	0.20

[a] M_n^{PS} and M_n^{PLA} were characterized by proton nuclear magnetic resonance (^{1}H NMR). [b] Polydispersity index (PDI) in the final diblock copolymers was determined by GPC using standard calibration. [c] $f_{PLA}^{v} = M_n^{PLA}/1.25/(M_n^{PLA}/1.25 + M_n^{PS}/1.04)$

assembly of PS-PLLA and polystyrene-*block*-poly(D-lactide) (PS-PDLA) BCP chains with opposite conformational chirality will give rise to formation of the H* phases (i.e., phase chirality) with opposite handedness as identified by transmission electron microscopy tomography, suggesting that the molecular chirality not only is the key factor to give the helical conformation but also controls the handedness of self-assembled morphology. A hypothetical mechanism with twisting and shifting instead of twisting and bending at the microphase-separated interface of the BCP* with the H* phase is thus proposed. To further investigate the shifting and twisting mechanism in the self-assembly of the BCPs*, a series of polylactide-containing BCPs with an achiral perylene moiety as a chemical junction was synthesized. As examined by CD and fluorescence experiments, significant induced CD (ICD) signals and a bathochromic shift of fluorescence emission for the achiral perylene moiety as a chemical junction of the BCPs* can be found only when the concentration of the BCPs* in toluene solution is higher than the critical micelle concentration (CMC), proving that the twisting and shifting mechanism is indeed initiated from the microphase-separated interface of the BCPs* via self-assembly. As a result, the optical activity of the ICD for the perylene moiety as a chemical junction in the BCP* can be directed by the helicity of the chiral entity in the polylactide-containing BCP*.

EXPERIMENTAL SECTION

Synthesis of Polylactide Homopolymers and Polylactide-Containing Block Copolymers. A typical ring-opening polymerization was used to prepare PLLA, PDLA, and poly(D,L-lactide) (PLA) homopolymers. The polydispersity (PDI) of synthesized polylactides was determined by GPC, and the number of lactide repeating units (N_{PLA}) was determined by ^{1}H NMR analysis (Table 1). ^{1}H NMR (500 MHz, $CDCl_3$): δ = 5.16 (q, 1H, CH(CH_3)), 1.58 (d, 3H, CH(CH_3)). PS-PLLA and PS-PDLA as well as polystyrene-*block*-poly(D,L-lactide) (PS-PLA) were prepared using two-step polymerization. Scheme 1 illustrates the synthetic routes of PS-PLLA. Double-headed initiator, 3-hydroxy-2,2-dimethylpropy-1,2-chloropropanoate, denoted as DHI4-Cl, was prepared. Hydroxyl-terminated polystyrene, PS−OH, was prepared by the bulk ATRP of styrene with DHI4-Cl as an initiator and CuBr/HMTETA as the catalyst/ligand. The molecular weight (M_n) and PDI of PS−OH were determined by GPC. BCPs were synthesized using the PS−OH as macroinitiator and $Sn(Oct)_2$ as a catalyst for typical ring-opening polymerization of lactides (see ref 15 for details). The PDI of the BCP was determined by GPC, and the number of LA repeating units (N_{PLA}) versus styrene repeating the units (N_{PS}) was determined by ^{1}H NMR analysis (Table 1). ^{1}H NMR

Scheme 1. Synthetic Routes of PS-PLLA

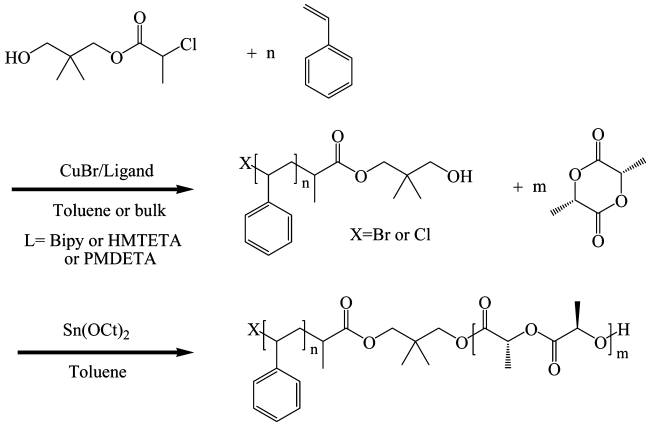

(500 MHz, $CDCl_3$): δ = 6.46−7.09 (br, 5H, ArH), 5.16 (q, 1H, C*H*(CH_3), J = 7.2 Hz), 1.84 (br, 1H, CH), 1.58 (d, 3H, CH(C*H*$_3$), J = 7.2 Hz), 1.42 (br, 2H, CH_2). The volume fractions of PLLA, PDLA, and PLA (f_{PLLA}^{v}, f_{PDLA}^{v}, and f_{PLA}^{v}) were calculated by assuming that the densities of polystyrene and enantiomeric polylactides are 1.02 and 1.25 g/cm^3 for PLLA and PDLA, respectively, and the density of PLA is 1.18 g/cm^3 for PLA.

Synthesis of Polylactide-Containing Block Copolymers with a Perylene Bisimide Junction. Scheme 2 illustrates the synthetic routes of PS-PLLA with a perylene bisimide junction (PS-*perylene*-PLLA). Detailed procedures for synthesis of PS-*perylene*-PLLA are described below. A mixture of asymmetric perylene with the anhydride group (compound **1** in Scheme 2), synthesized according to the method described by Nagao and co-workers,[20] amino-terminated PS (P3702-SNH$_2$: M_n = 32 000 g/mol and PDI = 1.04), and DMF were mixed in a round-bottom flask under nitrogen at room temperature. The mixture was sealed and heated to 150 °C in an oil bath and then remained at 150 °C for 8 h to yield hydroxy-terminated PS-perylene (compound **2** in Scheme 2). The resulting polymer was precipitated by adding methanol. The product was collected by vacuum filtration to give a pink powder and then dried under vacuum at 90−100 °C overnight to yield hydroxy-terminated PS-perylene. ^{1}H NMR (500 MHz, $CDCl_3$): δ = 8.6−8.8 (d, 8H, ArH of perylene), 6.46−7.09 (5H, ArH), 1.82 (backbone, 1H, CH), 1.40 (backbone, 2H, CH_2) (Figure S1, Supporting Information). Subsequently, the hydroxy-terminated PS-perylene (compound **2** in Scheme 2) can be used asa macroinitiator to react with L-lactide monomers using stannous(II) 2-ethyl hexanoate ($Sn(OCt)_2$) as catalyst for ring-opening polymerization (ROP), leading to formation of PS-*perylene*-PLLA (compound **3** in Scheme 2). ^{1}H NMR (500 MHz, $CDCl_3$): δ = 6.46−7.20 (5H, ArH), 5.12−5.16 (q, 1H, CH(CH_3)), 1.82 (backbone, 1H, CH), 1.58 (d, 3H,

dx.doi.org/10.1021/ja303513f | J. Am. Chem. Soc. 2012, 134, 10974−10986

Scheme 2. Synthetic Routes of PS-PLLA with a Perylene Bisimide Junction, PS-*perylene*-PLLA

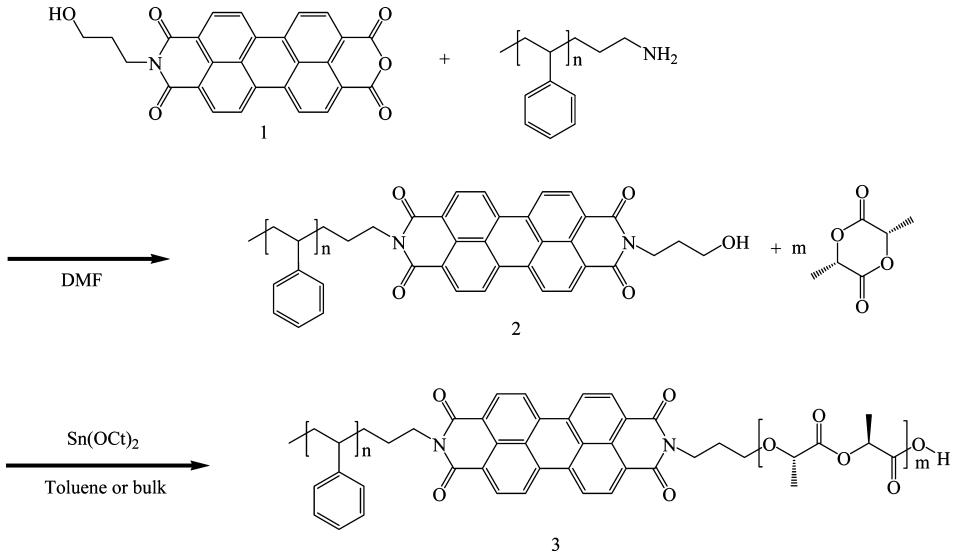

$CH(CH_3)$), 1.40 (backbone, 2H, CH_2) (Figure S5, Supporting Information). Also, similar routes were carried out to synthesize polystyrene-*perylene*-poly(D-lactide) (PS-*perylene*-PDLA) and polystyrene-*perylene*-poly(D,L-lactide) (PS-*perylene*-PLA). The PDI of the BCP was determined by GPC, and the number of LA repeating units (N_{PLA}) versus styrene repeating the units (N_{PS}) was determined by ^{1}H NMR analysis. Characterization data of the polylactide homopolymers, polylactide-containing BCPs, and polylactide-containing BCPs with a perylene bisimide junction is summarized in Table 1.

3D GPC Analysis for Polylactide-Containing BCPs with a Perylene Bisimide Junction. To further identify the polylactide-containing BCPs with a perylene bisimide junction, 3D GPC analyses,[21] consisting of an elution column equipped with a refractive-index detector and UV–vis spectra in series, were conducted. Figure S7a and S7b, Supporting Information, illustrates the 3D GPC analysis for PS-*perylene*-PLLA (f_{PLLA}^{v} = 0.35) and PS-PLLA (f_{PLLA}^{v} = 0.35), respectively. In contrast to PS-PLLA, where only the absorption bands of PS and PLLA around 220–300 nm can be observed, the absorption bands of the perylene moiety around 450–550 nm and the ones of PS and PLLA around 220–300 nm appear at approximately the same elution time. On the basis of the size exclusion effect of the GPC analysis, these results suggest that the perylene moiety indeed serves as the junction of PS-*perylene*-PLLA synthesized. Similar results were also observed from PS-*perylene*-PDLA (f_{PDLA}^{v} = 0.35) (Figure S7c, Supporting Information).

Sample Preparation. Bulk samples of PS-PLLA, PS-PDLA, and PS-PLA were prepared by solution casting from dichloromethane (CH_2Cl_2) at room temperature. Samples were first dissolved in CH_2Cl_2 at a concentration of 10 wt %. After the sample was completely dissolved in dichloromethane, the solution was filtrated through a filter with 0.45 μm pores to remove the impurities. The solution was then transferred in a vial and sealed well by aluminum foil having holes punched in for evaporation of the solvent. In order to minimize formation of defects and grain boundaries, the bulk samples can be obtained by solution casting from slow evaporation. Bulk samples were further dried in a vacuum oven for 3 days at 90 °C so as to remove the residual solvent. Subsequently, the dry samples were first heated to the annealing temperature at 175 °C for 3 min to eliminate the PLLA crystalline residues formed during the preparation procedure and then rapidly cooled at a rate of 150 °C/min to 140 °C for 3 h to stabilize the morphologies using a Perkin-Elmer DSC7 equipped with an Intracooler. Finally, the thermally treated samples were rapidly cooled at a rate of 150 °C/min to room temperature for further characterization.

Templated Sol–Gel Reaction. It is well known that aliphatic polyesters can be hydrolytically degraded because of the unstable character of the ester group.[22] Thermally treated samples of PS-PLLA and PS-PDLA were placed in a sodium hydroxide solution of methanol/water for 5 days to degenerate polylactides through hydrolysis. After hydrolysis, nanoporous PS with helical nanochannels can be prepared and used as a template for following the sol–gel reaction. To prepare the PS/SiO_2 helical nanohybrids, the SiO_2 precursor, tetraethoxysilane (TEOS), was introduced into the nanoporous PS template by immersing the template in a bottle of TEOS/$HCl_{(aq)}$(1M)/methanol mixture (weight ratio = 10/1/25) with a cap to avoid moisture at room temperature for 3 days. TEOS, $HCl_{(aq)}$, and methanol were used as SiO_2 precursor, catalyst, and solvent, respectively. For a successful pore-filling process in templated synthesis, appropriate solvents are required in order to enhance the wetting tendency of the precursor solution into the nanochannels of the template through capillary force. As a result, methanol was used as solvent for the precursor mixture so as to improve the wetting capability for the capillary-driven pore-filling process. After the pore-filling process of the precursor mixture, moisture was introduced into the bottle for initiation of the sol–gel reaction. The bottle without the cap was placed in an oven with controlled humidity at 50 °C for 2 days. Consequently, the pore-filled liquid precursor mixture can be transferred into a glassy solid (gels). After drying under atmosphere at 50 °C for 1 day, PS/SiO_2 helical nanohybrids can be prepared.

Characterization. Differential scanning calorimetry (DSC) experiments were carried out in a Perkin-Elmer DSC 7. The temperature and heat flow scales at constant heating rates (10 °C/min) were carefully calibrated using standard materials. DSC samples were first heated to the maximum annealing temperature, T_{max} = 180 °C, for 3 min in order to eliminate the crystalline residues of PLLA and PDLA formed during sample preparation. Those samples were then rapidly cooled at a rate of 150 °C/min to room temperature and heated again to T_{max} to examine T_g and T_m.

UV–vis absorption and CD spectra were acquired using a JASCO J-815 spectrometer. Fluorescence spectra were measured on Hitachi F-2500. Solution samples were placed in a cylindrical quartz cell with a light path of 1.0 mm. The concentration of the solution was 0.1 wt % for polylactide homopolymers and 0.025 wt % for polylactide-containing BCPs in acetonitrile (AcCN). FT-IR absorption and VCD spectra were acquired using a JASCO FVS-6000 spectrometer. Solution samples were placed in a cylindrical CaF_2 cell with a light path of 50 μm, whereas solid film samples were coated on a silicon wafer with a spin rate of 500 rpm. The concentration of the polymer solution was 2 wt % in CH_2Cl_2 and 5 wt % in 1,1,2-trichloroethane for spin coating. The Y axis of the absorption and circular dichroism spectra (i.e., molar concentration (M)) is normalized by the number of molecules in the polylactides synthesized.

dx.doi.org/10.1021/ja303513f | J. Am. Chem. Soc. 2012, 134, 10974–10986

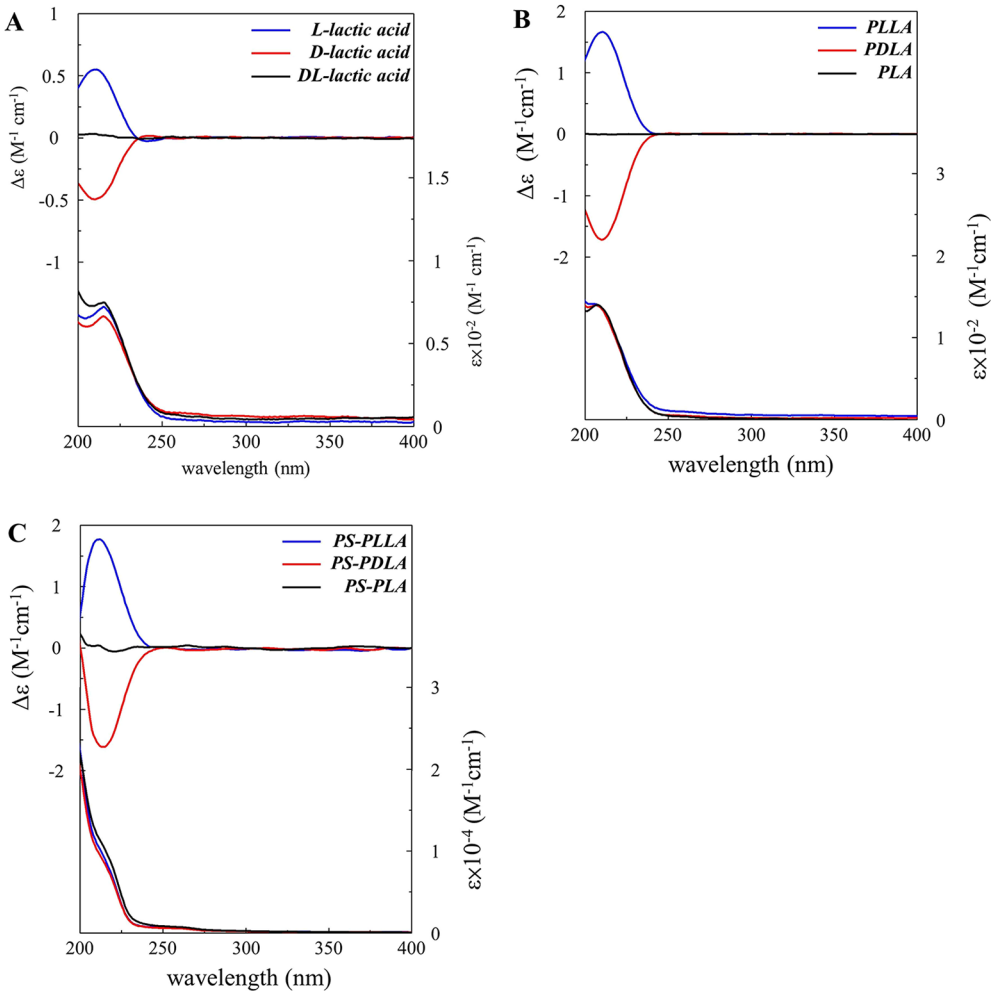

Figure 1. CD and corresponding UV−vis absorption spectra of (A) lactic acids, (B) polylactide homopolymers, and (C) polylactide-containing BCPs in dilute AcCN solution. Concentration of the solution is 0.1 wt %.

Bright-field transmission electron microscopy (TEM) images were obtained using a JEOL JEM-2100 LaB_6 transmission electron microscope (at an accelerating voltage of 200 kV). Bulk samples were sectioned at room temperature using a Leica Ultramicrotome (~100 nm in thickness). Then the microsections were collected on copper grids. Staining was accomplished by exposing the samples to the vapor of a 4% aqueous RuO_4 solution for 1 h to enhance the mass−thickness contrast under TEM observation.

Small angle X-ray scattering (SAXS) experiments were conducted at the synchrotron X-ray beamline 23A1 at the National Synchrotron Radiation Research Center (NSRRC) in Hsinchu, Taiwan. Bulk samples of the polylactide-containing BCP were first heated to the annealing temperature, T = 180 °C, for 3 min in order to eliminate the crystalline residues of PLLA and PDLA formed during sample preparation and then rapidly cooled at a rate of 150 °C/min to room temperature. All of the SAXS experiments were carried out at room temperature.

For TEM tomography (i.e., 3D TEM) experiments, the bulk samples of PS/SiO_2 helical nanohybrids fabricated using templates from PS-PLLA and PS-PDLA were first sectioned at room temperature using a Leica Ultramicrotome (~100 nm in thickness). Subsequently, the microsections were collected on copper grids (100 mesh) covered by a polyvinyl formal membrane. For the requirement of image alignment in the tomography, fiducial gold markers (diameter 10 nm, purchased from Polysciences, Inc.) were homogeneously distributed over the microsections. Subsequently, the samples were covered by a thin layer of carbon via vacuum sputtering to prevent radiation damage during collection of projections at different tilting angles. A series of 71 TEM images were collected from −70° to +70° tilt angles at an angular interval of 2° on a JEOL JEM-2100 LaB_6 transmission electron microscope operated at 200 kV. Images were recorded on a Gatan CCD camera. Alignment of the tilting series and 3D reconstruction were performed using IMOD software. The reconstructed volume was then filtered using a 7 × 7 × 7 median filter for noise reduction. Analyze 4.0 (AnalyzeDirect) was then used to trim the filtered volume, keeping only the volume of interest for further analysis.

RESULTS AND DISCUSSION

Conformational Chiralities of Polylactide Homopolymers and Polylactide-Containing BCPs. Figure 1A shows the CD and corresponding absorption spectra of L-lactic acid, D-lactic acid, and D,L-lactic acid in dilute acetonitrile (AcCN) solution. A positive CD signal from L-lactic acid and a negative one from D-lactic acid at 210 nm are found, and the characteristic absorption band is attributed to the $n \rightarrow \pi^*$ transition of carboxylate chromophore in the lactic acid. By contrast, the solution of D,L-lactic acid yields no CD signal. Figure 1B shows the CD and corresponding absorption spectra of PLLA, PDLA, and PLA in dilute AcCN solution. As in the spectroscopic results from enantiomeric lactic acids (Figure 1A), a positive CD signal from the PLLA and a negative one from the PDLA at 210 nm are found. Consistently, the solution of the PLA yields no CD signal. Notably, the intensities of the

dx.doi.org/10.1021/ja303513f | J. Am. Chem. Soc. 2012, 134, 10974−10986

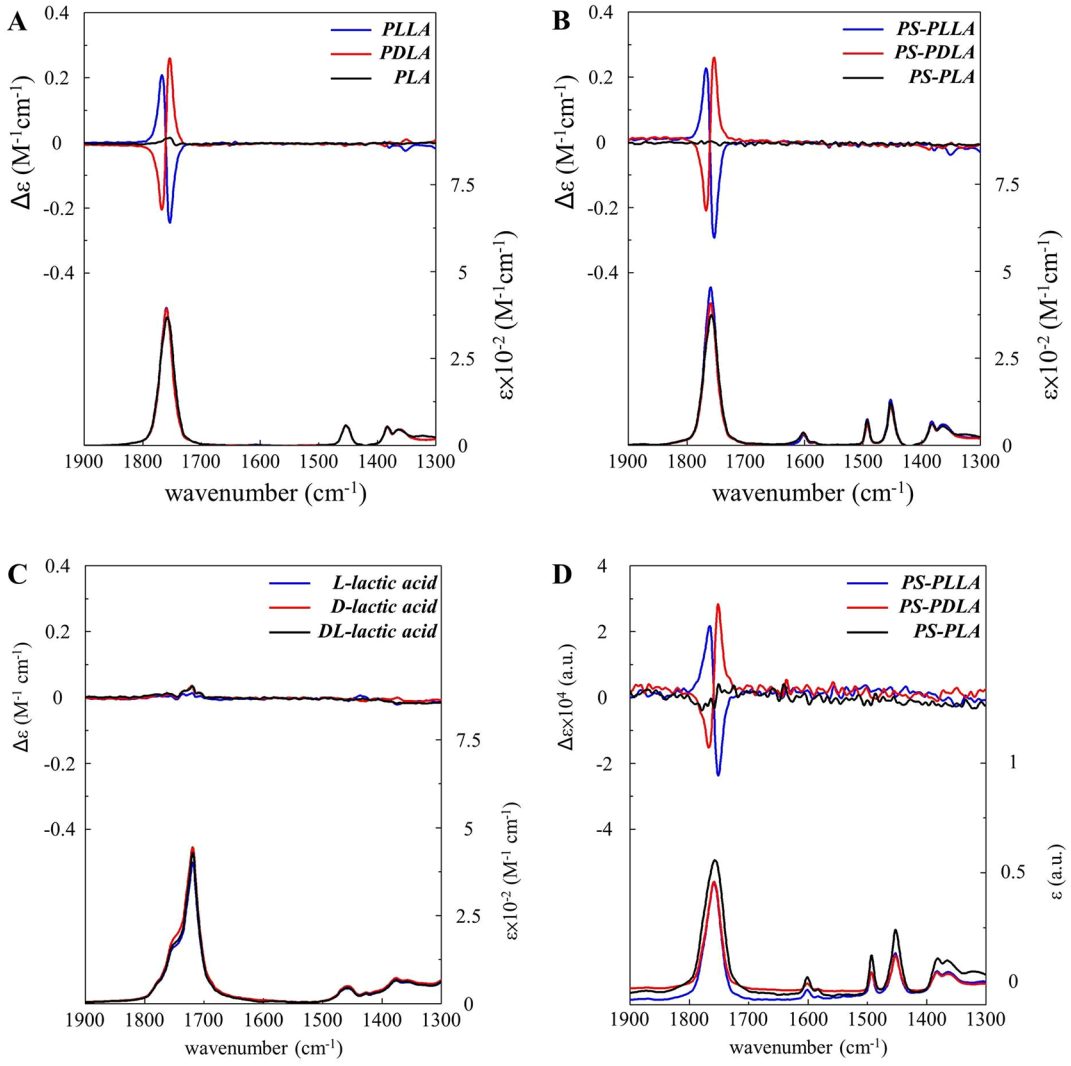

Figure 2. VCD and corresponding FT-IR absorption spectra of (A) polylactide homopolymers, (B) polylactide-containing BCPs, and (C) lactic acids in dilute CH_2Cl_2 solution. Concentration of the solution is 2 wt %. (D) VCD and corresponding FT-IR absorption spectra of polylactide-containing BCPs thin film.

CD signals from the PLLA and PDLA per chiral entity are approximately three times the absorption intensities of the L- and D-lactic acids per molecule, respectively. Restated, the optical activity of molecular chirality (configurational chirality) from lactic acid is amplified by formation of a helical conformation (conformational chirality) because of the transfer of chirality via the intramolecular interaction. The enhancement of CD intensity might be attributed to the phenomenon of chiral amplification.[23−27] Similarly, the opposite Cotton effects can be found from dilute solutions of PS-PLLA and PS-PDLA (Figure 1C). Consistently, the solution of PS-PLA yields no CD signal.

Note that the CD signals might result from anisotropic arrangement of the polymer chains at which the electric transition dipole (polarized along the C═O axis) of the carboxylate chromophore is perpendicular or parallel to the electric field of light.[28,29] To clarify the origins of the CD signals, LD measurements were performed. As shown in Figure S11, Supporting Information, no significant LD signals in the range from 200 to 250 nm can be found, indicating that the carboxylate chromophore of the polylactide chain in solution is intrinsically isotropic. These results suggest that significant CD signals of PLLA and PDLA are truly attributed to the interaction of chiral entities in polylactides and that the effect of anisotropic character is insignificant. Similarly, The absence of LD signals in the range from 200 to 250 nm for all of the polylactide-containing BCPs* (Figure S11c, Supporting Information) indicates that there is no severe anisotropic effect on spectroscopic measurements in such a dilute solution even with the existence of slight aggregation,[28,29] namely, the CD signals are truly contributed by the chiral entity in the constituted chiral blocks of the BCPs*.

On the basis of the Cotton effect appearing in the CD spectra, the absolute configurations of chiral monomers and chiral entities in chiral polymers can be identified. For helical polymers with an achiral conjugated backbone and chiral centers bonded to the side chain (i.e., side-chain chirality), CD spectroscopy can be used to investigate the handedness of the helical conformation by absorption of circularly polarized light (CPL).[30−33] However, for helical polymers with chiral entities on their polymer backbone (main-chain chirality), such as polylactides, the handedness of the helical conformation cannot be simply determined from the CD results because the $n \rightarrow \pi^*$ transition is relatively delocalized and can be significantly

dx.doi.org/10.1021/ja303513f | J. Am. Chem. Soc. 2012, 134, 10974−10986

affected by the neighboring chiral centers on the corresponding absorptions.[34] Notably, as compared to the electron transitions in CD, the absorptions that are attributed to molecular vibrational motions are less sensitive to the neighboring vibrational modes so that vibrational circular dichroism (VCD) can be utilized as a powerful tool in determining the handedness of the helical conformation of helical polymers with main-chain chirality.[35,36]

Figure 2A shows the VCD and corresponding absorption spectra of the PLLA, PDLA, and PLA in dilute dichloromethane (CH_2Cl_2) solution. For PLLA, a split-type Cotton effect with a negative VCD band at 1753 cm^{-1} and a positive one at 1767 cm^{-1} can be found. The inflection point at 1760 cm^{-1} corresponds to the characteristic absorption of the C═O stretching motion of the carbonyl group in polylactide. Consistently, the VCD spectrum of the PDLA appears as the mirror image of the spectrum of the PLLA, and the PLA solution yields no VCD signal. Similarly, dilute solutions of PS-PLLA and PS-PDLA exhibit opposite split-type Cotton effects (Figure 2B). On the basis of the coupled oscillator model and the signatures of the split-type Cotton effect in the VCD spectra,[37,38] the Cotton effect in the PLLA is identified as negative chirality whereas that in the PDLA is identified as positive chirality, namely, the helical conformation of the PLLA is left-handed and the PDLA must therefore exhibit a right-handed helical conformation. These results suggest that the BCPs* indeed have a polylactide block with preferential one-handed helical conformation. For comparison, VCD spectra of enantiomeric lactic acids and a racemic mixture in dilute CH_2Cl_2 solution were acquired (Figure 2C), and none of the lactic acids examined yields a significant VCD signal. As a result, the appearance of a split-type Cotton effect in the VCD spectra of the chiral polylactide blocks is indeed attributed to formation of a preferential one-handed helical conformation, resulting from the transfer of chirality from molecular chirality into conformational chirality due to intermolecular interaction.

3D Visualization of Helical Phase. To examine the microphase-separated morphologies from the self-assembly of the BCPs*, TEM and SAXS experiments were carried out. Figure 3A and 3C shows the 2D TEM projections of the helical phases formed by self-assembly of PS-PLLA and PS-PDLA, respectively. The RuO_4-stained PS microdomain appears as a dark matrix, whereas polylactide microdomains appear as bright helical nanostructures, revealing formation of the H* phase.[14,15] The corresponding 1D SAXS profiles show well-defined reflections at q^* ratios of $1:\sqrt{3}:\sqrt{4}:\sqrt{7}:\sqrt{13}$ in both BCPs* (Figure 3B and 3D), revealing that polylactide helical nanostructures are hexagonally packed in the PS matrix. In contrast to the BCPs* with the helical phase, the projection image of self-assembled PS-PLA and corresponding 1D SAXS profile (Figure 3E and 3F) suggest a typical hexagonally packed cylinder (HC) phase. Formation of the H* phase in the BCPs* suggests the effect of chirality on BCP self-assembly. To further examine whether formation of the H* phase is indeed attributed to the helical conformations of BCPs*, VCD experiments for the solid films of the BCPs* were carried out. Figure 2D shows the VCD and corresponding absorption spectra of the BCP* in solid film. In the VCD spectra, mirror-imaged VCD signals with a split-type Cotton effect for PS-PLLA and PS-PDLA can be found but PS-PLA is VCD silent. VCD results for the H* phases of the BCPs* (Figure 2D) are similar to those obtained from solution, suggesting that the

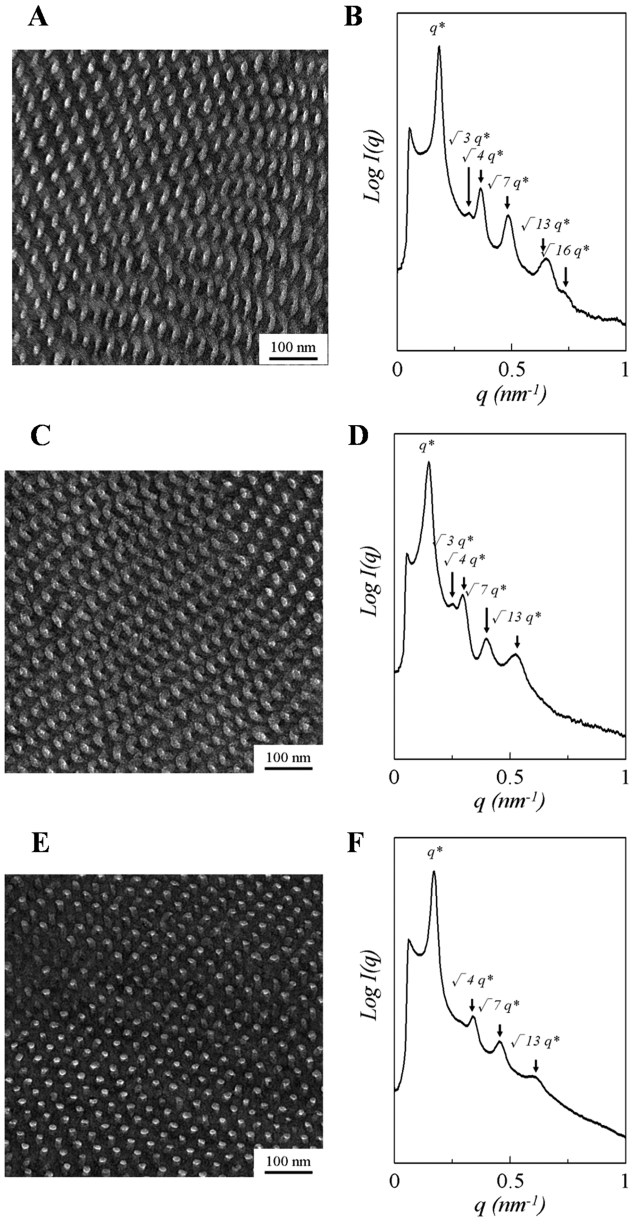

Figure 3. (A, C, E) TEM micrographs and (B, D, F) corresponding one-dimensional SAXS profiles of PS-PLLA, PS-PDLA, and PS-PLA, respectively.

BCP* chain in the H* phase indeed possesses preferentially a one-handed helical conformation.

Formation of the H* phase can be found in the self-assembly of the enantiomeric polylactide-containing BCPs* due to the effect of chirality. Considering the transfer of chirality from conformational chirality to phase chirality, it is intuitive to suggest that the forming helical phase will possess exclusive handedness through homochiral evolution. To examine the mechanism of homochiral evolution, identification of the handedness of the H* phase is essential. However, owing to the problem of imaging a 3D object using a 2D projection, the handedness of the helical phase cannot be directly determined by conventional TEM. After the microtoming of TEM sections, the helical nanostructure might be cut into half, resulting in ambiguous TEM projection for determining handedness (Figure S13, Supporting Information). To solve this problem, the H* phase should be directly visualized. As a result, TEM

dx.doi.org/10.1021/ja303513f | J. Am. Chem. Soc. 2012, 134, 10974−10986

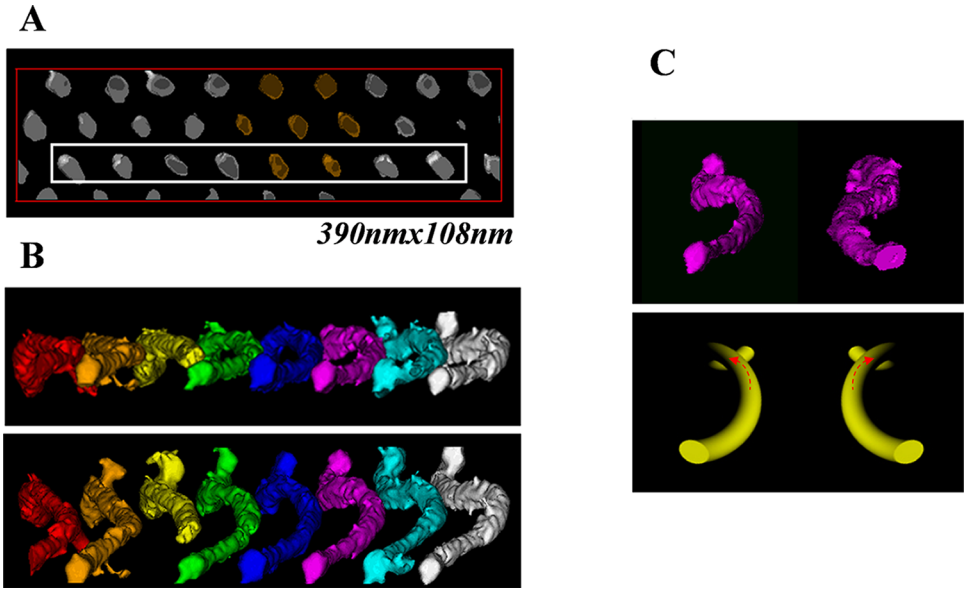

Figure 4. (A) 3D reconstruction of PS/SiO_2 helical nanohybrids fabricated using the template from PS-PLLA to undergo the sol–gel reaction. (B) 3D visualization of left-handed helical nanoarrays in the reconstructed volume of the rectangular area in Figure 4a, and use of color separation process to identify each helical microdomain. (C) Left-handed (left side) and right-handed (right side) helical nanostructures reconstructed from PS/SiO_2 helical nanohybrids fabricated using templates from PS-PLLA and PS-PDLA, respectively.

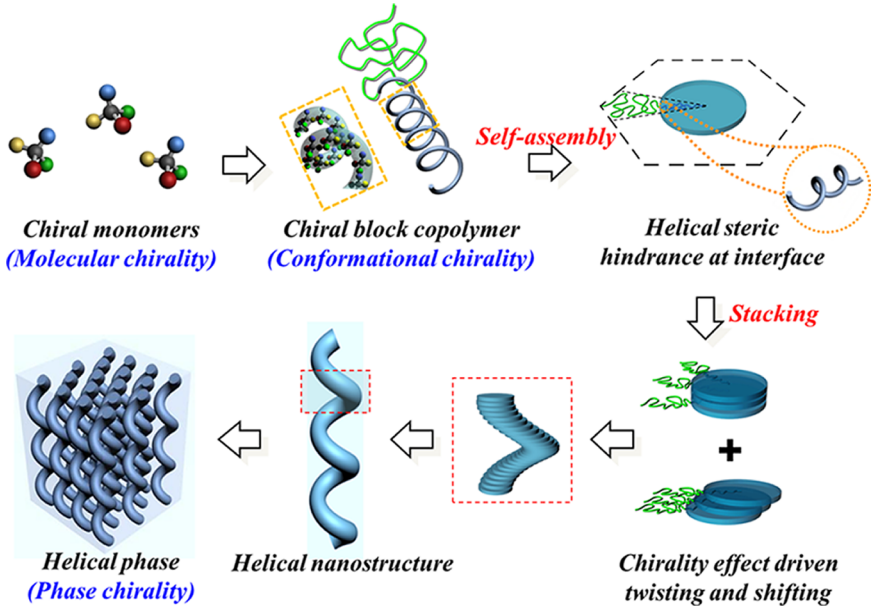

Figure 5. Schematic illustration of the hypothetical mechanism of transfer of chirality from molecular chirality into phase chirality in the self-assembly of BCPs*.

tomography was conducted to reconstruct the 3D images of the H* phase. However, there is a serious problem resulting from the staining of major phase for TEM projections. The RuO_4 stained matrix (i.e., dark PS microdomain) causes blocking of the contrast from the unstained minor phase (i.e., bright polylactide microdomains) at high tilt angle for projection, resulting in a low-contrast projection image. Moreover, RuO_4 is not a suitable staining agent for those BCPs* because of the diffusion problem for RuO_4 vapor resulting in unclear boundaries between PS and polylactide microdomains under TEM observation. Consequently, reconstruction from those low-contrast projection images cannot be binarized for 3D visualization. In order to change the mass–thickness contrast between PS and polylactide microdomians, a platform technology was developed to give the inverse mass–thickness contrast with better resolution in the projection for image reconstruction. This approach is to hydrolyze the polylactide blocks in the polylactide-containing BCPs*. Subsequently, nanoporous PS with hexagonally packed helical nanochannels can be fabricated and used as a template for the sol–gel process. Silica precursor mixture was introduced into the PS template by the pore-filling process. Well-defined helical nanohybrids with SiO_2 inorganic helices orderly dispersed in the PS matrix can be successfully obtained after the templated sol–gel process.[39]

Figure 4A shows the results of the 3D reconstruction of the PS/SiO_2 helical nanohybrids fabricated using the template from PS-PLLA to undergo the sol−gel reaction. These are consistent with the SAXS results (Figure S15a, Supporting Information), from which the hexagonal packing of nanohelices can be clearly identified. Figure 4B shows left-handed helical nanoarrays in the reconstructed volume of the rectangular area in Figure 4A, indicating the interdigitated character of the helical packing, as revealed by the use of a color separation process to identify each helical microdomain. Also, in Figure 4C, left-handed (left side) and right-handed (right side) helical nanostructures, reconstructed from PS/SiO_2 helical nanohybrids fabricated using templates from PS-PLLA and PS-PDLA, respectively, can be clearly identified. According to the reconstructed 3D TEM results, the handedness of the H* phase in PS-PLLA is preferentially left-handed whereas the handedness of the H* phase in PS-PDLA is right-handed, proving the homochiral evolution from conformational chirality to phase chirality in the self-assembly of the polylactide-containing BCPs* due to intermolecular interaction.

Origins for Forming Helical Phase. On the basis of the CD and VCD results and the reconstructed 3D TEM images of the H* phases from the polylactide-containing BCPs*, a hypothetical mechanism for the transfer of chirality from molecular chirality into phase chirality in the self-assembly of the BCPs* is proposed and presented in Figure 5. The chiral entity in the chiral polylactide block not only leads to formation of helical conformation but also determines the handedness of the helical conformation, inducing a preferential one-handed helical conformation via the intramolecular chiral interaction. By exploiting microphase separation resulting from intermolecular interaction, the chiral blocks in the BCP* segregate as a disk-shaped microdomain (platelet) from the achiral blocks based on the composition of the BCP*. Furthermore, by assuming that the number of PLLA chains comprising a microdomain is equal to the ratio of the microdomain volume (V_{domain}) to the molecular volume of a PLLA chain (v_{PLLA}), the number of PLLA chains within the microdomain (N) can thus be determined using the equation $N = V_{domain}/v_{PLLA} = S_{domain}/\sigma$. S_{domain} is the microdomain surface area. σ is the area at the surface of microdomain occupied by a single PLLA chain which can be replaced by $\sigma = 2v_{PLLA}/R_{PLLA}$ because the surface-to-volume ratio of the microdomain for the helix is $2/R_{PLLA}$.[40] R_{PLLA} is the radius of the PLLA microdomain and can be determined using the equation $R_{PLLA} = D \times (\sqrt{3} f_{PLLA}^{v}/2\pi)^{0.5}$. D is the interdomain spacing, determined by the primary peak of the SAXS profile. Also, v_{PLLA} can be replaced by $v_{PLLA}\ M_{PLLA}/(\rho_B \times N_{Av})$. M_{PLLA} is the molar mass of the PLLA chain, N_{Av} is Avogadro's number, and ρ_B is the density of the PLLA chain. M_{PLLA} is 15 600 g/mol, and ρ_B is 1.25 g/cm^3. The calculated result of v_{PLLA} is 20.80 nm^3, and σ is 3.37 nm^2 for the helical phase. Furthermore, the number of PLLA chains within the microdomain can be described as $N = (\pi \times R_{PLLA}^2 \times \sqrt{\sigma})/v_{PLLA}$.[41] Accordingly, the number of PLLA chains within the microdomain is approximately 42, and the angle between two adjacent PLLA chains within the microdomain is approximately 8.6°. The calculated helical pitch length is 142 nm, and the area at the surface of the microdomain occupied by a single PLLA chain is 3.37 nm^2, namely, the interdistance between the stacking microdomains is approximately 1.84 nm. Consequently, the number of microdomains (platelet) within one helical pitch length is 77, so that the twisting angle between stacking microdomains in the helical phase is calculated as approximately 4.7°. Subsequently, owing to the effect of specific helical steric hindrance on molecular packing and microdomain stacking, each disk-shaped microdomain will twist and shift toward the others during morphological evolution from self-assembly. Furthermore, the chemical junctions of constituent blocks will be induced to orient at the microphase-separated interface so as to yield helical curvature at the interface. The increase in the interfacial area between PS and polylactide microdomains is associated with the enthalpic penalty that arises from incompatibility. This enthalpic penalty could be balanced by formation of a partially ordered state in the polylactide microdomains resulting from the intermolecular chiral interaction. This process reduces the Gibbs free energy of the system. Moreover, owing to the homochiral evolution, the polylactide microdomains are stacked in a preferred direction along the central axis of the nanohelix, giving the nanohelix a preferential handedness. Eventually a well-defined helical phase with hexagonally packed polylactide nanohelices in a PS matrix will be formed based on the volume fraction of the space in the PS matrix that is filled by the constituent polylactide.

Evidence for Twisting at the Microphase-Separated Interface. To investigate the suggested mechanism in the self-assembly of the BCPs*, a series of polylactide-containing BCPs with an achiral perylene moiety as a chemical junction was synthesized (See Experimental Section for details). Note that the optical activity of the achiral moiety can be induced by introducing chiral dopants through noncovalent bonding association or covalent bonding of the achiral moiety with chiral entities; the behavior is referred to as the Pfeiffer effect or induced circular dichroism (ICD).[42−47] As a result, on the basis of the suggested twisting mechanism, the ICD of the achiral perylene moiety as a chemical junction of the polylactide-containing BCPs* is expected due to introduction of a chiral block for microphase separation. Figure 6 shows the CD and corresponding absorption spectra of polylactide-containing BCPs with a perylene junction in toluene solution. From PS-*perylene*-PLLA (f_{PLLA}^{v} = 0.21), the negative CD signals at 518,

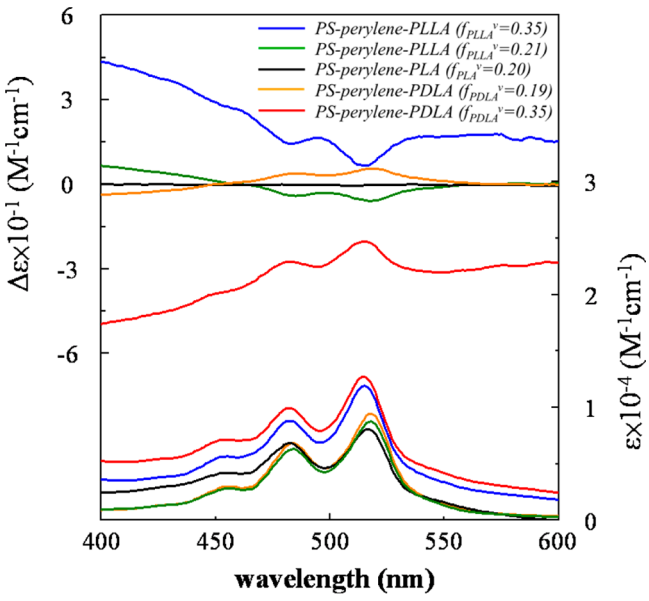

Figure 6. CD and corresponding UV−vis absorption spectra of polylactide-containing BCPs with a perylene junction in toluene solution. Concentration of the solution is 2 wt %.

dx.doi.org/10.1021/ja303513f | J. Am. Chem. Soc. 2012, 134, 10974−10986

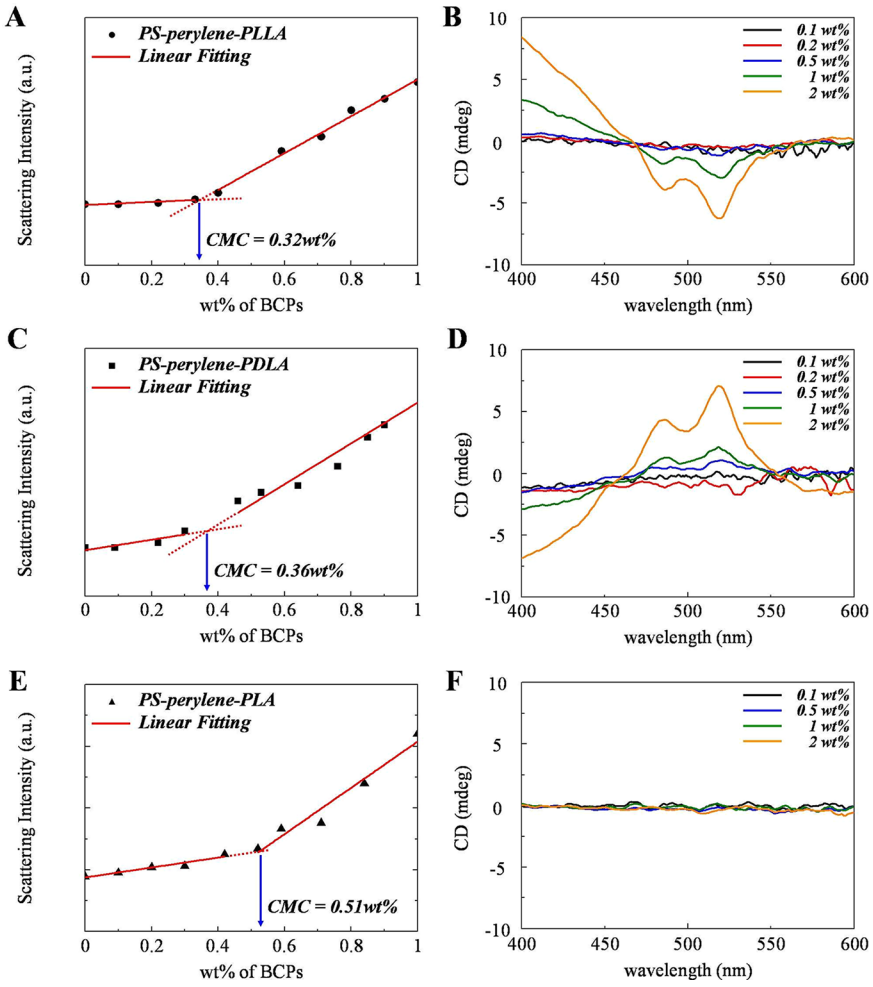

Figure 7. (A, C, E) Critical micelle concentration (CMC) measurements by light scattering (He−Ne laser, λ = 632 nm) at T = 20 °C and (B, D, F) corresponding concentration-dependent CD spectra of PS-*perylene*-PLLA (f_{PLLA}^{v} = 0.21), PS-*perylene*-PDLA (f_{PDLA}^{v} = 0.19), and PS-*perylene*-PLA (f_{PLA}^{v} = 0.20) in toluene solution, respectively.

484, and 454 nm are attributed to the characteristic absorption bands of the achiral perylene moiety[48] and a positive broadening band between 300 nm and the visible spectral region can be identified. Consistently, the spectrum of PS-*perylene*-PDLA (f_{PDLA}^{v} = 0.19) appears as a mirror image of the spectrum of PS-*perylene*-PLLA (f_{PLLA}^{v} = 0.21), and there is no optical activity for PS-*perylene*-PLA (f_{PLA}^{v} = 0.20) in solution due to the lack of a preferential one-handed helical conformation. Furthermore, the CD signals of PS-*perylene*-PLLA (f_{PLLA}^{v} = 0.21) and PS-*perylene*-PDLA (f_{PDLA}^{v} = 0.19) from 300 nm to the visible spectral region suggest long-range scattering, which is attributed to formation of self-assembled optically active aggregates (see below for reasons).[49,50] Similarly, the opposite Cotton effect can be found in toluene solutions of PS-*perylene*-PLLA (f_{PLLA}^{v} = 0.35) and PS-*perylene*-PDLA (f_{PDLA}^{v} = 0.35). As observed, the signs of the ICD signals attributed to the characteristic absorption bands of the achiral perylene moiety correspond well with the chiralities of chiral blocks in the BCPs*. Furthermore, the intensities of the ICD signals from the achiral perylene moiety increase with increasing volume fraction of chiral block in BCPs* and reach a maximum for the one with the composition for forming helical phase. As a result, we speculate that the induced optical activity of molecular chirality from the perylene moiety can be amplified by formation of helical curvature resulting from microphase separation.

To further investigate the ICD signals driven by the self-assembly of the BCPs*, the concentration-dependent CD spectra of polylactide-containing BCPs with a perylene junction in toluene solution were acquired. As toluene is a selective solvent for the PS, micellization will occur once the concentration of BCP reaches the critical micelle concentration (CMC). The CMCs of PS-*perylene*-PLLA (f_{PLLA}^{v} = 0.21), PS-*perylene*-PDLA (f_{PDLA}^{v} = 0.19), and PS-*perylene*-PLA (f_{PLA}^{v} = 0.20) were determined as approximately 0.32, 0.36, and 0.51 wt %, respectively (Figure 7). Notably, the CMC value of the BCP* is obviously lower than the racemic one, indicating that the chiral interaction induced by the intermolecular packing of chiral polymer chains significantly increases the incompatibility between achiral PS and chiral blocks in the BCPs*. In contrast to PS-*perylene*-PLA (Figure 7F) at which no CD signal can be recognized even with the concentration over the CMC, the CD signals of the enantiomeric BCPs* appear once the concentration is higher than the CMC (Figure 7B and 7C). For comparison, the concentration-dependent CD spectra of PS-*perylene*-PLLA in a neutral solvent, CH_2Cl_2, was also acquired. As shown in Figure S18, Supporting Information, the CD is silent even with high concentration since there is no occurrence of microphase separation at the prepared

dx.doi.org/10.1021/ja303513f | J. Am. Chem. Soc. 2012, 134, 10974−10986

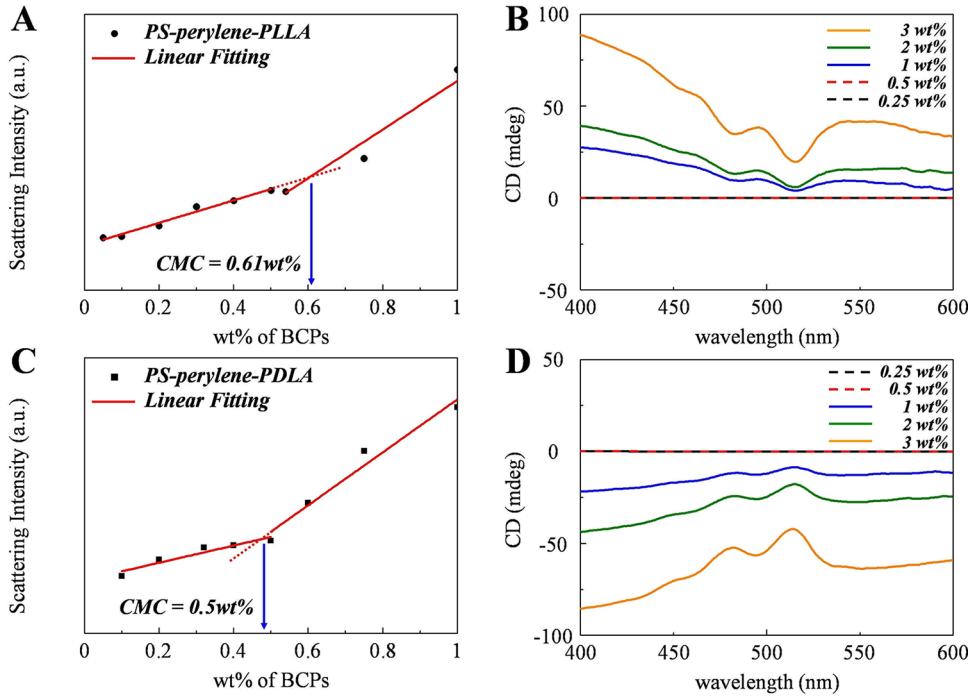

Figure 8. (A, C) Critical micelle concentration measurements by light scattering (He−Ne laser, λ = 632 nm) at T = 20 °C and (B, D) corresponding concentration-dependent CD spectra of PS-*perylene*-PLLA (f_{PLLA}^{v} = 0.35) and PS-*perylene*-PDLA (f_{PDLA}^{v} = 0.35) in toluene solution, respectively.

concentrations. Accordingly, those results suggest that the ICD indeed results from self-assembly of BCP composed of chiral entities. Similar results can also be observed in PS-*perylene*-PLLA (f_{PLLA}^{v} = 0.35) and PS-*perylene*-PDLA (f_{PDLA}^{v} = 0.35) (Figure 8).

As the self-assembly of BCPs* is driven by noncovalent bonding forces, the ICD is expected to be dependent upon temperature. To examine the effect of temperature on the ICD, CD spectra of the BCPs* with a perylene junction in toluene solution were acquired at different temperatures. Figure S19, Supporting Information, shows temperature-dependent CD spectra of PS-*perylene*-PLLA (f_{PLLA}^{v} = 0.21) in toluene solution at which a decrease in the intensity of ICD signals upon increasing temperature can be clearly observed and eventually go silent at high temperature. Moreover, the ICD signals appear again after cooling from high temperature, reflecting that the ICD behavior is indeed a reversible process (i.e., a typical character of self-assembling process). Accordingly, the ICD signals are driven by self-assembly of BCPs*, as revealed by examination of the critical micelle concentration (CMC) and the corresponding self-assembling behavior of the BCP* in solution. Therefore, the ICD results suggest twisting at the microphase-separated interface of the BCPs* by self-assembly.

As demonstrated by the ICD results above, the optical activity of the ICD for the perylene moiety as a chemical junction in the BCP* can be directed by the helicity of the chiral entity in the polylactide-containing BCP*. To identify the handedness of the chiral block in the polylactide-containing BCP* with a perylene junction, VCD experiments were carried out. Figure 9 shows the VCD and corresponding absorption spectra of the polylactide-containing BCPs with a perylene junction in toluene solution. For PS-*perylene*-PLLA (f_{PLLA}^{v} = 0.21), a split-type Cotton effect with a negative VCD band at 1740 cm^{-1} and a positive one at 1767 cm^{-1} can be found; the results are similar to that of PLLA and PS-PLLA (Figures 2A and 2C). Consistently, the VCD spectrum of PS-*perylene*-PDLA

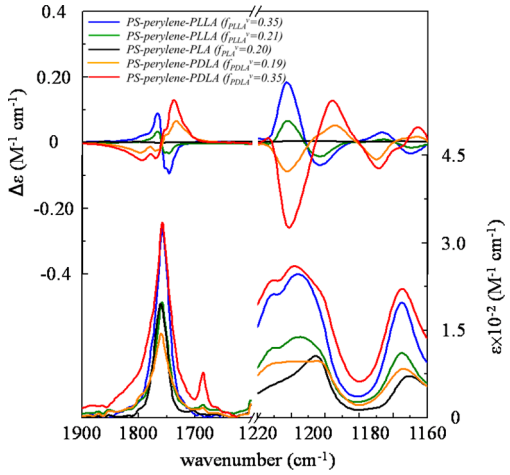

Figure 9. VCD and corresponding FT-IR spectra of polylactide-containing BCPs with a perylene junction in toluene. Concentration of solution is 2 wt %.

(f_{PDLA}^{v} = 0.19) appears as the mirror image of the spectrum for PS-*perylene*-PLLA. By contrast, the solution of PS-*perylene*-PLA yields no VCD signal. Similarly, an opposite split-type Cotton effect can be found in toluene solutions of PS-*perylene*-PLLA (f_{PLLA}^{v} = 0.35) and PS-*perylene*-PDLA (f_{PDLA}^{v} = 0.35), namely, the helical conformation of PLLA in PS-*perylene*-PLLA is left-handed, and PDLA in PS-*perylene*-PDLA should possess a right-handed helical conformation. Similar to the results from the polylactide-containing BCPs*, the BCPs* with a perylene junction indeed possess polylactide block with preferential one-handed helical conformation. Notably, the absorption bands of the C−O−C vibrations in the range from 1120 to 1220 cm^{-1} for PS-*perylene*-PDLA and PS-*perylene*-PDLA are broader than the absorption bands of the C−O−C vibrations for PS-*perylene*-PLA, indicating that there exists much more complicated C−

dx.doi.org/10.1021/ja303513f | J. Am. Chem. Soc. 2012, 134, 10974−10986

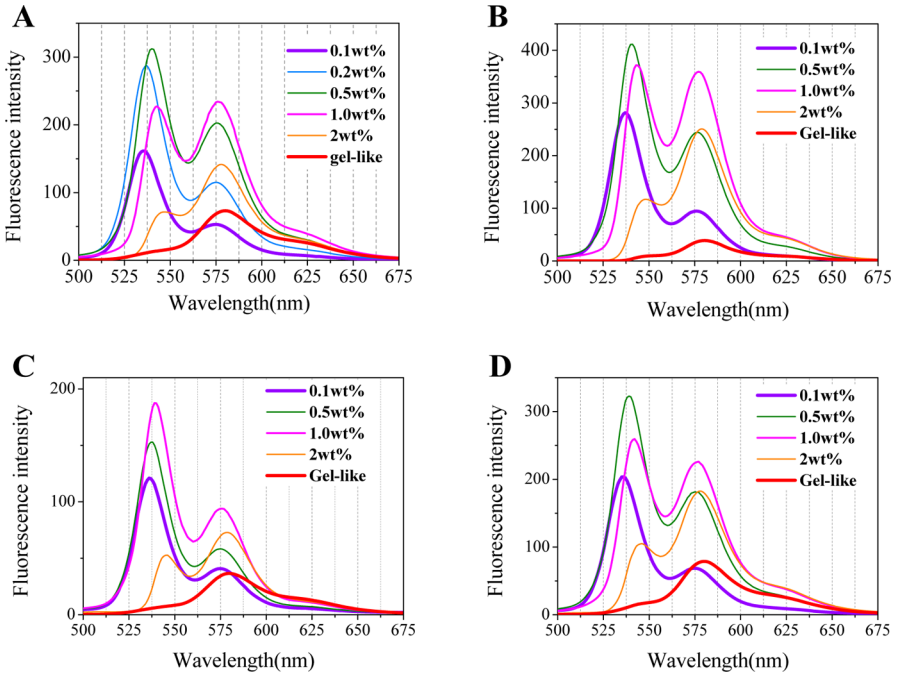

Figure 10. Concentration-dependent fluorescence spectra of (A) PS-*perylene*-PLLA (f_{PLLA}^{ν} = 0.35), (B) PS-*perylene*-PDLA (f_{PDLA}^{ν} = 0.35), (C) PS-*perylene*-PLLA (f_{PLLA}^{ν} = 0.21), and (D) PS-*perylene*-PDLA (f_{PDLA}^{ν} = 0.19) in toluene solution. Wavelength for excitation is 450 nm.

O−C vibration modes in the enantiomeric polylactide-containing BCPs* than that in the racemic one.[35] The results may suggest that the intermolecular interaction of the chiral blocks did occur in the BCPs* with a perylene junction leading to an increase in the C−O−C vibration modes from chiral interaction.

To further examine the origins of the split-type VCD results, concentration-dependent VCD spectra of the BCPs* were acquired. As shown in Figure S20, Supporting Information, the VCD signals in the absorption bands of the C−O−C vibration appear once the concentration of BCPs* is higher than the CMC whereas the VCD signals in the absorption bands of the C═O vibration can be observed even with the concentration lower than the CMC (e.g., 0.1 wt %). On the basis of the coupled oscillator approximation,[34] the electron transition dipoles of the C−O−C vibration are almost parallel to the helical axis of chiral blocks but the electron transition dipole of the C═O vibration is perpendicular to the helical axis of the chiral blocks. As a result, the VCD results are in line with the suggested intermolecular interaction resulting from self-assembly of the chiral polymer chain in the BCPs* at which molecular packing gives rise to the appearance of VCD signals in the absorption bands of the C−O−C vibration. For comparison, the VCD spectra of the BCPs* were also acquired in CH_2Cl_2 (a neutral solvent) solution; the VCD signals in the absorption bands of C−O−C vibration appear silent in CH_2Cl_2 solution, as expected (Figure S21, Supporting Information). Moreover, the absorption bands of the C−O−C vibration in toluene solution are broader than that in CH_2Cl_2 solution and undergo a hypsochromic shift (i.e., blue shift) (Figure S21, Supporting Information). These results further suggest that the intermolecular interaction of the chiral blocks did occur in the BCP* self-assembly. Accordingly, the homochiral evolution from molecular chirality to hierarchical chirality via formation of the conformation chirality of the chiral chain corresponds well with the ICD behavior of the achiral perylene moiety as the junction of the BCPs*.

Evidence for Shifting at the Microphase-Separated Interface. On the basis of the ICD results driven by the self-assembly of the BCPs* with a perylene junction, the twisting mechanism can be clearly evidenced. Nevertheless, as illustrated in Figure 5, the origins for forming helical phase (i.e., microdomain with helical curvature) should involve the twisting and shifting mechanism. According to the suggested twisting and shifting mechanism, the shifting mechanism should result in interesting fluorescence emission at which the type of aggregation for the perylene junctions will give rise to obvious differences between the one with shifting (J aggregation) and the one without shifting (H aggregation). Figure 10A shows the concentration-dependent fluorescence spectra of PS-*perylene*-PLLA (f_{PLLA}^{ν} = 0.35) in toluene solution. As the BCP concentration increases, the maximum emission peak gradually shifts from 535 ($\nu' = 0 \rightarrow \nu = 0$) to 571 nm ($\nu' = 0 \rightarrow \nu = 1$), where ν and ν' are the vibrational quantum numbers of the ground and excited states,[51] respectively, revealing that the perylene moieties begin to self-assemble into aggregates.[51−53] Most interestingly, the emission peaks also undergo a bathochromic shift. Once the BCP concentration exceeds the CMC, the bathochromic shifting becomes significant and the emission intensity sharply declines. These results suggest that the perylene moieties preferentially form a slipped $\pi-\pi$-stacked J aggregation by self-assembly.[54] Similar results were also observed from PS-*perylene*-PDLA (f_{PDLA}^{ν} = 0.35) (Figure 10B). The emission results therefore suggest shifting associated with the perylene moieties in the aggregated state by self-assembly.

Similar ICD (Figure 7) results can be obtained from the self-assembly of the BCPs* with compositions in the HC phase region. However, the results of fluorescence emission from the HC phase slightly differ from those in the helical phase; the bathochromic shift from the HC phase (Figure 10C and 10D) is less significant than that in the H* phase, suggesting that the

dx.doi.org/10.1021/ja303513f | J. Am. Chem. Soc. 2012, 134, 10974−10986

proportion of J aggregation in the HC phase of the BCP* is much lower than that from the H* phase (Figure 10C and 10D). Accordingly, most of the chemical junctions of the BCPs* in the HC phase are arranged in a twisting manner at the microphase-separated interface. This observation suggests that the helical steric hindrance did change the manner of packing from self-assembly. Owing to the effect of chirality on molecular packing and microdomain stacking, the chiral blocks in the BCP* segregate as a disk-shaped microdomain from the achiral blocks based on the composition of the BCP*, as illustrated in Figure 5. Subsequently, for development of the H* phase, the disk-shaped microdomain will twist and shift toward the others during morphological evolution from self-assembly, resulting in formation of microdomain with helical curvature. By contrast, for development of the HC phase, the disk-shaped microdomain will mainly twist only toward the others while the perylene junctions of constituent blocks are still oriented at the microphase-separated interface but with the twisting mechanism (a nonconventional way for allocation of the chemical junctions in BCP self-assembly).

CONCLUSIONS

In this work, a methodology for studying the transfer of chirality at different length scales is developed to elucidate insights into morphological evolution from the molecular level. The molecular chirality of lactic acids, polylactide homopolymers, and polylactide-containing BCPs* can be determined using CD which yields a positive Cotton effect for L-lactic acid, PLLA, and PS-PLLA and a negative Cotton effect for D-lactic acid, PDLA, and PS-PDLA. VCD can be used to investigate the handedness of the helical conformation; the split-type VCD spectrum with negative chirality suggests preferential left-handed helical conformations of PLLA homopolymer and the PLLA block in PS-PLLA but positive chiralities for PDLA homopolymer and the PDLA block in PS-PDLA. Direct visualization of helical phases using TEM tomography clearly reveals formation of left- and right-handed helical nanostructures in the PS matrix in PS-PLLA and PS-PDLA, respectively. The significant ICD of the achiral perylene moiety as a chemical junction of the BCPs* driven by microphase separation suggests the occurrence of twisting at the microphase-separated interface of the BCPs*, while the bathochromic shift of fluorescence results suggests the occurrence of shifting at the interface. The twisting and shifting mechanism thus leads to formation of the H* phase in the enantiomeric polylactide-containing BCPs* from self-assembly and also decides the handedness of forming H* phase by stacking the chiral polymer chains in a preferred direction along the central axis of the nanohelix, giving the nanohelix a preferential handedness. Accordingly, homochiral evolution from molecular chirality to phase chirality can be demonstrated in the self-assembly of the enantiomeric polylactide-containing BCPs* via the twisting and shifting mechanism.

ASSOCIATED CONTENT

Supporting Information

Synthesis, characterization, and other experimental details of BCP with polylactide-containing BCPs with a perylene bisimide junction, and characterization of polylactide homopolymers and polylactide-containing BCPs. This material is available free of charge via the Internet at http://pubs.acs.org.

AUTHOR INFORMATION

Corresponding Author

E-mail: rmho@mx.nthu.edu.tw

Notes

The authors declare no competing financial interest.

ACKNOWLEDGMENTS

The authors would like to thank the National Science Council of the Republic of China, Taiwan, for financially supporting this research under Contract No. NSC 100-2120-M-007-013.

REFERENCES

(1) Lehn, J. M. *Science* **1985**, *227*, 849.
(2) Whitesides, G. M.; Grzybowski, B. *Science* **2002**, *295*, 2418.
(3) Creighton, T. E. *Proteins: Structure and Molecular Principles*; Freeman: New York, 1983.
(4) Hirschberg, J. H. K. K.; Brunsveld, L.; Ramzi, A.; Vekemans, J. A. J. M.; Sijbesma, R. P.; Meijer, E. W. *Nature* **2000**, *407*, 167.
(5) Cornelissen, J. J. L. M.; Rowan, A. E.; Nolte, R. J. M.; Sommerdijk, N. A. J. M. *Chem. Rev.* **2001**, *101*, 4039.
(6) Green, M. M.; Nolte, R. J. M.; Meijer, E. W. *Topics in Stereochemistry*; Denmark, S. E., Siegel, J., Eds.,; Wiley: Hoboken, NJ, 2003; Vol. *24* (Materials-Chirality).
(7) Tomar, S.; Green, M. M.; Day, L. A. *J. Am. Chem. Soc.* **2007**, *129*, 3367.
(8) Ho, R.-M.; Chiang, Y.-W.; Lin, S. C.; Chen, C.-K. *Prog. Polym. Sci.* **2011**, *36*, 376.
(9) Thomas, E. L.; Anderson, D. M.; Henkee, C. S.; Hoffman, D. *Nature* **1988**, *334*, 598.
(10) Bates, F. S.; Fredrickson, G. H. *Annu. Rev. Phys. Chem.* **1990**, *41*, 525.
(11) Chen, J. T.; Thomas, E. L.; Ober, C. K.; Mao, G. P. *Science* **1996**, *273*, 343.
(12) Bates, F. S.; Fredrickson, G. H. *Phys. Today* **1999**, *52*, 32.
(13) Cornelissen, J. J. L. M.; Fischer, M.; Sommerdijk, N. A. J. M.; Nolte, R. J. M. *Science* **1998**, *280*, 1427.
(14) Ho, R.-M.; Chiang, Y.-W.; Tsai, C.-C.; Lin, C.-C.; Ko, B.-T.; Huang, B.-H. *J. Am. Chem. Soc.* **2004**, *126*, 2704.
(15) Ho, R.-M.; Chiang, Y.-W.; Chen, C.-K.; Wang, H.-W.; Hasegawa, H.; Akasaka, S.; Thomas, E. L.; Burger, C.; Hsiao, B. S. *J. Am. Chem. Soc.* **2009**, *131*, 18533.
(16) Lehn, J. M. *Supramolecular Chemistry: Concepts and Perspectives*; VCH: New York, 1995.
(17) Orr, G. W.; Barbour, L. J.; Atwood, J. L. *Science* **1999**, *285*, 1049.
(18) Engelkamp, H.; Middelbeek, S.; Nolte, R. J. M. *Science* **1999**, *284*, 785.
(19) de Jong, J. J. D.; Lucas, L. N.; Kellogg, R. M.; van Esch, J. H.; Feringa, B. L. *Science* **2004**, *304*, 278.
(20) Nagao, Y.; Naito, T.; Abe, Y.; Misono, T. *Dyes Pigm.* **1996**, *32*, 71.
(21) Wu, X.; Fraser, C. L. *Macromolecules* **2000**, *33*, 4053.
(22) Zalusky, A. S.; Olayo-Valles, R.; Wolf, J. H.; Hillmyer, M. A. *J. Am. Chem. Soc.* **2002**, *124*, 12761.
(23) Green, M. M.; Andreola, C.; Mufioz, B.; Reidy, M. P. *J. Am. Chem. Soc.* **1988**, *110*, 4063.
(24) Green, M. M.; Peterson, N. C.; Sato, T.; Teramoto, A.; Cook, R.; Lifson, S. *Science* **1995**, *268*, 1860.
(25) Green, M. M.; Reidy, M. P.; Johnson, R. J.; Darling, G.; O'Leary, D. J.; Willson, G. *J. Am. Chem. Soc.* **1989**, *111*, 6452.
(26) Jha, S. K.; Cheon, K.-S.; Green, M. M.; Selinger, J. V. *J. Am. Chem. Soc.* **1999**, *121*, 1665.
(27) Green, M. M.; Garetz, B. A.; Munoz, B.; Chang, H.; Hoke, S.; Cooks, R. G. *J. Am. Chem. Soc.* **1995**, *117*, 4181.
(28) Shindo, Y.; Ohmi, Y. *J. Am. Chem. Soc.* **1985**, *107*, 91.
(29) Rodger, A.; Nordén, B. *Circular Dichroism and Linear Dichroism*; Oxford University Press Ltd.: New York, 1997.

(30) Yashima, E.; Maeda, K.; Nishimura, T. *Chem.—Eur. J.* **2004**, *10*, 42.
(31) Yashima, E.; Maeda, K. *Macromolecules* **2008**, *41*, 3.
(32) Fujiki, M. *Macromol. Rapid Commun.* **2001**, *22*, 539.
(33) Fujiki, M. *Top. Curr. Chem.* **2008**, *284*, 119.
(34) Schwartz, E.; Domingos, S. R.; Vdovin, A.; Koepf, M.; Buma, W. J.; Cornelissen, J. J. L. M.; Rowan, A. E.; Nolte, R. J. M.; Woutersen, S. *Macromolecules* **2010**, *43*, 7931.
(35) Nafie, L. A.; Keiderling, T. A.; Stephens, P. J. *J. Am. Chem. Soc.* **1976**, *98*, 2715.
(36) Nafie, L. A.; Diem, M. *Acc. Chem. Res.* **1979**, *12*, 296.
(37) Nakanishi, K.; Berova, N.; Woody, R. W. *Circular Dichroism: Principles and Applications*; VCH Press Ltd.: New York, 1994.
(38) Holzwarth, G.; Chabay, I. *J. Chem. Phys.* **1972**, *57*, 1632.
(39) Tseng, W.-H.; Chen, C.-K.; Chiang, Y.-W.; Ho, R.-M. *J. Am. Chem. Soc.* **2009**, *131*, 1356.
(40) Tcherkasskaya, O.; Ni, S.; Winnik, M. A. *Macromolecules* **1996**, *29*, 4241.
(41) Tanaka, H.; Hasegawa, H.; Hashimoto, T. *Macromolecules* **1990**, *23*, 4378.
(42) Mason, S. F.; McCaffery, A, J. *Nature (London)* **1964**, *204*, 468.
(43) Falk, H.; Jungwirth, W.; Müller, N. *Monatsh. Chem.* **1984**, *115*, 455.
(44) Borovkov, V. V.; Hembury, G. A.; Inoue, Y. *Angew. Chem., Int. Ed.* **2003**, *42*, 5310.
(45) Yashima, E.; Matsushima, T.; Okamoto, Y. *J. Am. Chem. Soc.* **1995**, *117*, 11596.
(46) Yashima, E.; Matsushima, T.; Okamoto, Y. *J. Am. Chem. Soc.* **1997**, *119*, 6345.
(47) Yang, S. Y.; Green, M. M.; Schultz, G.; Jha, S. K.; Müller, A. H. E. *J. Am. Chem. Soc.* **1997**, *119*, 12404.
(48) Birks, J. B.; Dyson, D. J. *Proc. R. Soc., London* **1963**, *A275*, 135.
(49) Bustamante, C.; Tinoco, I., Jr.; Maestreo, M. F. *Proc. Natl. Acad. Sci. U.S.A.* **1983**, *80*, 3568.
(50) Schnur, J. M.; Ratna, B. R.; Selinger, J. V.; Singh, A.; Jyothi, G.; Easwaran, K. R. K. *Science* **1994**, *264*, 945.
(51) Wang, W.; Han, J. J.; Wang, L. Q.; Li, L. S.; Shaw, W. J.; Li, A. D. Q. *Nano Lett.* **2003**, *3*, 455.
(52) Würthner, F.; Thalacker, C.; Sautter, A. *Adv. Mater.* **1999**, *11*, 754.
(53) Würthner, F.; Thalacker, C.; Sautter, A.; Schärtl, W.; Ibach, W.; Hollricher, O. *Chem.—Eur. J.* **2000**, *6*, 3871.
(54) Würthner, F.; Thalacker, C.; Diele, S.; Tschierske, C. *Chem.—Eur. J.* **2001**, *7*, 2245.